

Sparse Generalized Multiscale Finite Element Methods and their applications

Eric Chung* Yalchin Efendiev† Wing Tat Leung‡ Guanglian Li§

September 25, 2021

Abstract

In a number of previous papers [20, 23, 21, 4, 12, 13, 11, 10], local (coarse grid) multi-scale model reduction techniques are developed using a Generalized Multiscale Finite Element Method. In these approaches, multiscale basis functions are constructed using local snapshot spaces, where a snapshot space is a large space that represents the solution behavior in a coarse block. In a number of applications (e.g., those discussed in the paper), one may have a sparsity in the snapshot space for an appropriate choice of a snapshot space. More precisely, the solution may only involve a portion of the snapshot space. In this case, one can use sparsity techniques ([6, 5, 7, 38, 44, 37]) to identify multiscale basis functions. In this paper, we consider two such sparse local multiscale model reduction approaches.

In the first approach (which is used for parameter-dependent multiscale PDEs), we use local minimization techniques, such as sparse POD, to identify multiscale basis functions, which are sparse in the snapshot space. These minimization techniques use l_1 minimization to find local multiscale basis functions, which are further used for finding the solution. In the second approach (which is used for the Helmholtz equation), we directly apply l_1 minimization techniques to solve the underlying PDEs. This approach is more expensive as it involves a large snapshot space; however, in this example, we can not identify a local minimization principle, such as local generalized SVD.

All our numerical results assume the sparsity and we discuss this assumption for the snapshot spaces. Moreover, we discuss the computational savings provided by our approach. The sparse solution allows a fast evaluation of stiffness matrices and downscaling the solution to the fine grid since the reduced dimensional solution representation is sparse in terms of local snapshot vectors. Numerical results are presented, which show the convergence of the proposed method and the sparsity of the solution.

*Department of Mathematics, The Chinese University of Hong Kong, Shatin, Hong Kong SAR. Eric Chung's research is partially supported by CUHK Direct Grant for Research 2014-15.

†Department of Mathematics and Institute for Scientific Computation (ISC), Texas A&M University, College Station, Texas 77843-3368, USA

‡Department of Mathematics and Institute for Scientific Computation (ISC), Texas A&M University, College Station, Texas 77843-3368, USA. This work is partially supported by the U.S. Department of Energy Office of Science, Office of Advanced Scientific Computing Research, Applied Mathematics program under Award Number DE-FG02-13ER26165

§Institute for Numerical Simulation, the University of Bonn, Wegelerstrasse 6, 53115 Bonn, Germany

1 Introduction

1.1 Multiscale problems and the problem of sparsity

Simulations of multiscale problems are expensive and, typically, require some type of a model reduction. Our approaches seek adaptive reduced-order models, locally in space, and construct multiscale basis functions in each coarse region to represent the solution space. These approaches share common concepts with homogenization and upscaling methods [42, 2, 22, 46, 28, 30, 25, 24], where local effective properties are constructed. In contrast, in multiscale methods, local multiscale basis functions [33, 36, 39, 22, 40, 16, 15, 29, 14, 17, 24, 48, 34] are constructed to represent the solution space. These basis functions are typically constructed in the snapshot spaces [20]. In this paper, we investigate cases, when the basis functions are sparse in the snapshot space. We discuss several examples, which include multiscale parameter-dependent problems and the Helmholtz equation. The parameter-dependent multiscale problems are motivated by stochastic problems, where the parameter is used to describe the uncertainties.

1.2 Sparse GMsFEM Concepts

In this paper, we use the GMsFEM framework ([27, 26, 23, 21, 4, 12, 13, 11, 10, 20]) and investigate the sparsity within GMsFEM snapshots. To illustrate the main idea of our approach, we consider

$$Lu = f,$$

where L is a differential operator. For example, in the paper, we consider parameter-dependent heterogeneous flows, $Lu = -\text{div}(\kappa(x; \mu)\nabla u)$, and the Helmholtz equation, $Lu = -\text{div}(\kappa(x)\nabla u) - \Omega^2 n(x)u$. The main idea of GMsFEM is to construct a snapshot space and identify a subspace, called the offline or online space depending whether the problem is parameter-dependent. This subspace is used to solve the underlying problem at a reduced cost. The snapshot and online spaces are constructed in each coarse element (see next section for more precise definitions), where a coarse element is a region, which is much larger than the characteristic fine-length scale (see Figure 2). For each coarse region, τ_j , we construct snapshot vectors, $\{\psi_i^j\}$ (here i is the numbering of the snapshot functions), that represent the local solution space. We denote the snapshot space by

$$V_{\text{snap}}^{\tau_j} = \text{Span}_i\{\psi_i^j\}, \quad V_{\text{snap}} = \text{Span}_{i,j}\{\psi_i^j\}.$$

In GMsFEM, the online spaces are constructed using the elements of local snapshot functions. In many examples, the snapshot space can be large and the online space can be a sparse subspace of the snapshot space. The objective of this paper is to investigate these cases.

1.3 Snapshot spaces

The snapshot spaces play an important role in the GMsFEM. They are designed to capture the solution space locally and are used to preserve some features of the solution space, e.g., mass conservation. Typical snapshot spaces consist of local solutions constructed using some sets of boundary conditions or right hand sides. With an appropriate choice of snapshot spaces (e.g., using oversampling [21]), one can improve the convergence of GMsFEM substantially.

To convey the concept of snapshot spaces, we present some examples. We will consider two examples discussed above. We start with a simplified example related to the parameter-dependent

case, $L_0 u = -\text{div}(\kappa(x; \mu = 0)\nabla u)$, i.e., the problem without a parameter. In each coarse-grid block τ_j (see the left plot in Figure 2), we consider a local solution

$$L_0(\psi_i^j) = 0 \text{ in } \tau_j \quad (1)$$

subject to some boundary conditions, where these boundary conditions play an important role in defining snapshot functions. One option is to choose all possible boundary conditions considering all unit vectors on the boundary of τ_j . More precisely, $\psi_i^j(x) = \delta_i(x)$ on $\partial\tau_j$, where $\delta_i(x)$ is 1 at the node i and zero elsewhere. The computations of these snapshot functions are expensive. Instead, we use the boundary conditions, which are randomly distributed numbers on the fine-grid nodes of the boundary $\partial\tau_j$ (see the left plot in Figure 2). The random boundary conditions allow extracting the essential information provided we choose several more snapshot vectors than the number of modes, we would like to use. For *parameter-dependent problems*, the snapshot vectors are defined as above (1) for each pre-selected value of μ_m . For example, for *one-dimensional case* $\tau_j = [x_j, x_{j+1}]$, for parameter-independent problem, the snapshot space in τ_j consists of two solutions ψ^j and ψ^{j+1} , such that $\psi^n(x_l) = \delta_{nl}$, $n = j, j+1$, $l = j, j+1$, where δ_{jl} is the Kronecker symbol and ψ^n ($n = j, j+1$) is a solution of $\frac{d}{dx}(\kappa(x; \mu = 0)\frac{d}{dx}\psi^n) = 0$ in τ_j (see Figure 1 for illustration). For *parameter-dependent problems*, the snapshot vectors in $\tau_j = [x_j, x_{j+1}]$ are the solutions of

$$\frac{d}{dx} \left(\kappa(x; \mu_m) \frac{d}{dx} \psi_m^n \right) = 0 \text{ in } \tau_j,$$

$\psi_m^n(x_l) = \delta_{nl}$, $n = j, j+1$, $l = j, j+1$. For multi-dimensional examples, we can construct the snapshots similarly for each τ_j and for using different boundary conditions and use one index to represent the snapshot vectors as ψ_i^j . For the second example, $Lu = -\text{div}(\kappa(x)\nabla u) - \Omega^2 n(x)u$, we choose the snapshot vectors to be functions $e^{i\Omega k_i x}$ for a set of pre-defined values of k_i on a unit circle (see the right plot in Figure 2).

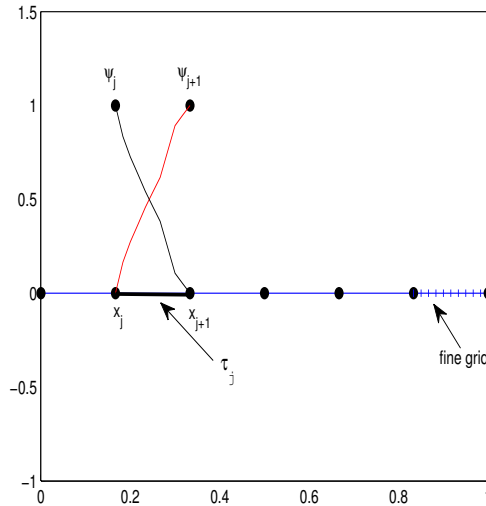


Figure 1: Illustration of snapshot concepts in one dimensional example.

The multiscale basis functions are constructed in the snapshot space. Our earlier approaches seek a small dimensional subspace of the snapshot space by performing a local spectral decomposition (based on analysis). However, these approaches use all snapshot vectors when seeking multiscale basis functions. In a number of applications, the solution is sparse in the snapshot space. I.e., in the expansion

$$u = \sum_{i,j} c_{i,j} \psi_i^j,$$

many coefficients $c_{i,j}$ are zeros. In this case, one can save computational effort by employing sparsity techniques. In this paper, our main goal is to discuss how GMsFEM can be designed if the solution is sparse in the snapshot space. We describe two classes of approaches and present a framework for constructing sparse GMsFEM.

The main challenge in these applications is to construct a snapshot space, where the solution is sparse. In our first example, this can be achieved, because an online parameter value μ can be close to some of the pre-selected offline values of μ 's, and thus, the multiscale basis functions (and the solution) can have a sparse representation in the snapshot space. In our second example, we select cases where the solution u contains only a few snapshot vectors corresponding to directions k_i . We note that if the snapshot space is not chosen carefully, one may not have the sparsity. In general, there can be many other examples and our goal is to show how local multiscale model reduction techniques can be used for such problems.

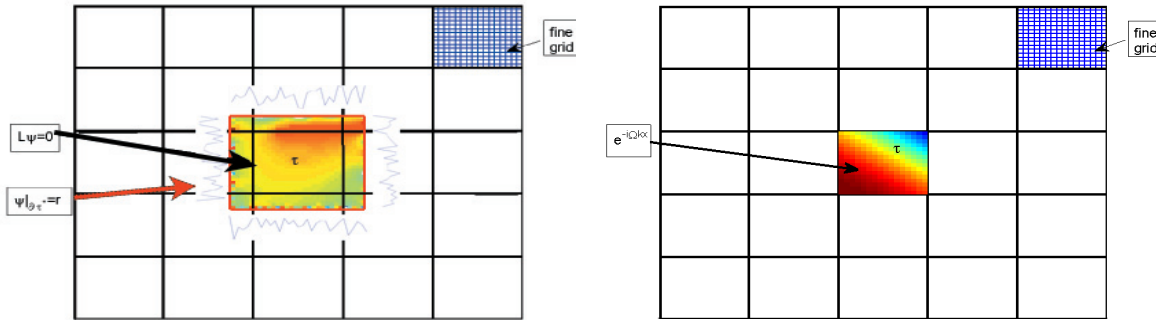


Figure 2: Illustration of snapshot concepts. Left: For the first problem; Right: For the second problem.

1.4 Approaches for identifying sparse solutions in snapshot spaces

The main goal of this paper is to discuss how to explore sparsity ideas within GMsFEM for constructing local multiscale basis functions. We consider two distinct cases.

- First approach: “Local-Sparse Snapshot Subspace Approach”. Determining the online sparse space locally via local spectral sparse decomposition in the snapshot space (motivated by parameter-dependent problems).
- Second approach: “Sparse Snapshot Subspace Approach”. Determining the online space globally via a global solve (motivated by using plane wave snapshot vectors and the Helmholtz equation).

See Figure 3 for illustration. We use sparsity techniques (e.g., [6, 5, 7, 38, 44]) to identify local multiscale basis functions and solve the global problem.

In above approaches, the snapshot functions can be linearly dependent. In fact, in general, we would like to have a large snapshot space that can contain a sparse representation of the solution. In both approaches formulated above, the linear dependency is removed. In the first approach, it is removed by sparse POD. We note that in the original GMsFEM approach [20], POD across all snapshot functions is used to remove linear dependence. However, this can result in a loss of sparsity, i.e., the solution may contain many nonzero coefficients when represented in the snapshot space. Thus, for sparsity, it is important to avoid a POD step across all snapshot vectors. In our first example, we need to avoid using POD for all μ 's. For this reason, we design a special sparse POD method using randomized snapshot functions. It both eliminates linearly dependent snapshot functions and identifies a sparse solution space. In the second method, l_1 minimization can be used for all snapshots, even if they are linearly dependent. By adding more snapshot vectors, we hope to identify a sparse representation of the solution. The second method will eliminate the linear dependence and identify a sparse solution. Note that in our example, the snapshot vectors are linearly independent.

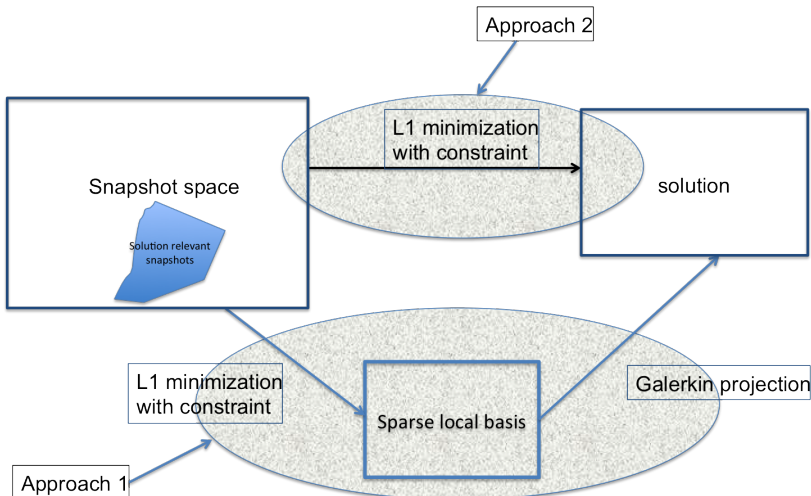


Figure 3: Illustration of our approaches.

For the first case, we consider parameter-dependent elliptic equations of the form

$$-\operatorname{div}(\kappa(x; \mu) \nabla u) = f \text{ in } D, \quad (2)$$

where $u = g$ on ∂D , and μ is a parameter. Some of the existing approaches for parameter-dependent problems closely related to the proposed approaches include reduced basis techniques [3, 8]. In these approaches, the reduced order model is constructed via a greedy algorithm. In the proposed approach, we attempt to approximate the solution space locally in each coarse block using l_1 minimization. Local multiscale basis functions are constructed using GMsFEM. In previous approaches, we attempted to compress the local solutions corresponding to some pre-selected values, μ , in the offline stage. This can lead to large dimensional offline spaces. In this paper, we propose an approach to compute eigenvectors using l_1 minimization based on randomized snapshots and oversampling. This provides an efficient approach to identify sparse eigenvector representation in

GMsFEM. The proposed approach gives a sparse representation of the multiscale basis functions in terms of the snapshot space vectors and has several advantages. (1) It allows quickly assembling of the stiffness matrix in the online space since it involves a few elements of the snapshot space. (2) We can downscale the solution to the fine grid much faster using sparse representation. (3) It avoids a POD based step proposed in the original GMsFEM formulation (see [20]), which is performed across all μ 's and which can result to a large dimensional representation of the online multiscale basis functions in terms of snapshot functions.

In the second example, we consider the Helmholtz equation

$$-\operatorname{div}(\kappa(x)\nabla u) - \Omega^2 n(x)u = f \text{ in } D, \quad (3)$$

where Ω is the frequency. We will use plane waves as the snapshot vectors. In the computational examples considered in this paper, the solution has a few dominant propagating directions, and is, therefore, spanned by only a few plane waves. This observation leads to the solution sparsity in our snapshot space. However, the choice of local spectral decomposition is not available for determining these dominant directions and we study using l_1 minimization directly in the space of snapshot vectors. We consider not very large snapshot spaces, and snapshot vectors having closed form formulas for constant media properties ($\kappa(x)$ and $n(x)$). For the Helmholtz equation (3) with low frequencies, we can expect a sparsity in our examples, which we exploit. Thus, sparsity techniques are the natural methodologies in these situations. In general, we can also consider the frequency to be a parameter, and apply similar techniques used for the first example.

1.5 Summary of numerical results

Two test cases for the first approach are presented, where we consider parametrized conductivity fields. In the first case, the conductivity is parametrized as an affine combination of two heterogeneous conductivity fields. In the second case, we use a nonlinear parameter dependence. In particular, we consider an initial conductivity field with a channel and inclusions. The parametrization is introduced such that these high-conductivity features spatially move within the domain. This is a more challenging example because high-conductivity features appear in many parts of the domain. Numerical results show that our approach provides an accurate approximation of the solution using a few degrees of freedom and the solution is sparse in an appropriate snapshot space.

Numerical results for the second approach involve solving the Helmholtz equation in media with two isolated heterogeneous inclusions. We consider a domain with two distinct properties, where plane wave solutions can provide a good approximation. In this case, the solution is spanned by only a few plane waves, and is, therefore, sparse in the space of plane waves with many propagating directions. However, in general, we do not know which plane wave directions are dominant and our algorithm identifies these directions by using l_1 minimization.

The paper is organized in the following way. In the next section, we present preliminaries and discuss GMsFEM, coarse and fine grid concepts. In Section 3, we propose our new construction for the online space. Section 4 is devoted to numerical results. In Section 5, we present conclusions.

2 Preliminaries

To discretize (2) or (3), we let \mathcal{T}^H be a usual conforming partition of the computational domain D into finite elements (triangles, quadrilaterals, tetrahedrals, etc.) and \mathcal{E}^H denotes all the edges

in the coarse mesh \mathcal{T}^H . We refer to this partition as the coarse grid and assume that each coarse subregion is partitioned into a connected union of fine-grid blocks. The fine-grid partition will be denoted by \mathcal{T}^h . We use $\{x_i\}_{i=1}^{N_v}$ (where N_v denotes the number of coarse nodes) to denote the vertices of the coarse mesh \mathcal{T}^H , and define the neighborhood of the node x_i by

$$\omega_i = \bigcup \{K_j \in \mathcal{T}^H; \quad x_i \in \bar{K}_j\}. \quad (4)$$

See Figure 4 for an illustration of neighborhoods and elements subordinated to the coarse discretization. We emphasize the use of ω_i to denote a coarse neighborhood, and K to denote a coarse element throughout the paper.

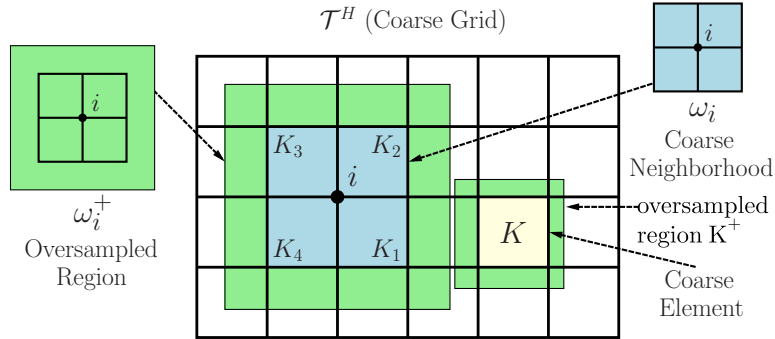


Figure 4: Illustration of a coarse neighborhood and coarse element

Next, we briefly outline the global coupling and the role of coarse basis functions for the respective formulations that we consider. For the discontinuous Galerkin (DG) formulation, we use a coarse element K as the support for basis functions, and for the continuous Galerkin (CG) formulation, we use ω_i as the support of basis functions. In turn, throughout this chapter, we use the notation

$$\tau_i = \begin{cases} \omega_i & \text{for CG} \\ K_i & \text{for DG} \end{cases} \quad (5)$$

when referring to a coarse region where respective local computations are performed (see Figure 4). To further motivate the coarse basis construction, we offer a brief outline of the global coupling. In particular, we note that our approach will employ multiple basis functions per coarse neighborhood. Both CG and DG solutions will be sought as $u_{\text{ms}}^{\text{DG/CG}}(x; \mu) = \sum_{i,k} c_k^i \psi_k^{\tau_i}(x; \mu)$, where $\psi_k^{\tau_i}(x; \mu)$ are the basis functions (without loss of generality, we write basis functions as parameter-dependent). Once the basis functions are identified, the global coupling is given through the variational form

$$a_{\text{DG/CG}}(u_{\text{ms}}^{\text{DG/CG}}, v; \mu) = (f, v), \quad \text{for all } v \in V_{\text{on}}^{\text{DG/CG}}, \quad (6)$$

where $V_{\text{on}}^{\text{DG/CG}}$ is used to denote the space formed by those basis functions and $a_{\text{DG/CG}}$ is a bilinear form which will be defined later on. Throughout, for the convenience, we use the same notations for the discrete and continuous representations of spatial fields.

3 Sparse GMsFEM

In this section, we will give the detailed constructions of our sparse GMsFEM. We start with an outline of the approach.

3.1 Outline

In this section, we present an outline of the algorithm. Assume that the snapshot space is $V_{\text{snap}}^\tau = \text{Span}\{\psi_i^{\text{snap}}\}$ for a generic element τ . We assume that the solution is sparse in this snapshot space and consider two approaches (see Figure 3 for illustration). Throughout the paper, we will assume that the solution is sparse in the snapshot space. We will discuss the assumption on the sparsity later in Section 5.

General outline of the sparse GMsFEM:

1. Coarse grid generation.
2. Construction of snapshot space, where the solution is sparse.
3.
 - *First approach. Local-Sparse Snapshot Subspace Approach.* Seek a subspace of the snapshot space and construct multiscale basis functions that are sparse in the snapshot space.
 - *Second approach. Sparse Snapshot Space Approach.* Solve for the sparse solution in the snapshot space directly within a global formulation.

In the first approach, we perform local calculations to identify multiscale basis functions that are sparse in the snapshot space. Here, we will use approaches similar to sparse POD. Then, the global problem is solved in the space of multiscale basis functions. The resulting solution is sparse.

In the second approach, we apply directly sparse solution techniques and find the solution that is sparse in the snapshot space. This approach is more expensive since it uses a large snapshot space. However, in some examples, we can not identify local basis functions in the offline stage and such approaches give sparse solutions in the online stage.

3.2 First approach. Local-Sparse Snapshot Subspace Approach

We first give a general idea of this approach. We consider a local snapshot space $V_{\text{snap}}^\tau = \text{Span}\{\psi_i^{\text{snap}}\}$. In the local snapshot space, we seek multiscale basis functions $\{\psi_i^{\text{on}}\}$ that are sparse in the local snapshot space and which have smallest energies (similar to sparse POD). For example, following to [44], we can consider

$$\min_{\Psi \in \mathbb{R}^{n \times M_{\text{on}}^\tau}} \frac{1}{\nu} \|\Psi\|_1 + \text{Tr}\langle \Psi^T A_s(\mu) \Psi \rangle, \text{ s.t. } \Psi^T \Psi = \mathbf{I},$$

where n is the dimension of the fine-scale space, M_{on}^τ is the number of online basis functions and $A_s(\mu)$ is the stiffness matrix formed in the snapshot space. Our proposed local approach avoids expensive direct local eigenvalue calculations and uses randomized snapshots. This approach will be used for problems where one knows a local basis construction principle. The latter typically uses some local generalized eigenvalue problems in the snapshot spaces [44]. Once multiscale basis functions (that are sparse in the snapshot space) are constructed, we solve the problem on a coarse grid.

Here, we will consider the parameter-dependent problem (2). We can consider the computation of the parameter-dependent coarse space as an online procedure. In the latter, our objective will be solving many problems for a given value of the parameter with different boundary conditions and the right hand sides.

3.2.1 Snapshot space

We first construct a snapshot space V_{snap}^τ (for a generic τ). Construction of the snapshot space involves solving the local problems for various choices of input parameters, and we describe it below. We generate snapshots using random boundary conditions by solving a small number of local problems imposed with random boundary conditions,

$$\begin{aligned} -\text{div}(\kappa(x; \mu_j) \nabla \psi_{l,j}^{\tau, \text{rsnap}}) &= 0 \quad \text{in } \tau^+ \\ \psi_{l,j}^{\tau, \text{rsnap}} &= r_l \quad \text{on } \partial\tau^+, \end{aligned} \tag{7}$$

where r_l are independent identically distributed (i.i.d.) standard Gaussian random vectors on the fine-grid nodes of the boundary, $l = 1, \dots, L$. μ_j ($j = 1, \dots, J$) is a specified set of fixed parameter values, and J denotes the number of parameter values we choose. Here, τ^+ is an oversampled region shown in the Figure 4 as ω_i^+ or K^+ for conforming Galerkin formulation or discontinuous Galerkin formulation.

The space generated by $\psi_{l,j}^{\tau, \text{rsnap}}$ is a subspace of the space generated by all local snapshots $\Psi_{k,j}^{\tau, \text{snap}}$, $k = 1, \dots, N$, and N denotes the number of boundary nodes. Denote $\Psi_j^{\tau, \text{rsnap}} = [\psi_{1,j}^{\tau, \text{rsnap}}, \dots, \psi_{L,j}^{\tau, \text{rsnap}}]$ and $\Psi_j^{\tau, \text{snap}} = [\psi_{1,j}^{\tau, \text{snap}}, \dots, \psi_{N,j}^{\tau, \text{snap}}]$. Therefore, for each parameter μ_j , there exists a randomized matrix \mathcal{R} with rows composed by the random boundary vectors r_l (as shown in Equation (7)), such that,

$$\Psi_j^{\tau, \text{rsnap}} = \mathcal{R} \Psi_j^{\tau, \text{snap}}. \tag{8}$$

Now, we are ready to present the local snapshot space as follows,

$$V_{\text{snap}}^\tau = \text{Span}\{\psi_{l,j}^{\tau, \text{rsnap}} : 1 \leq j \leq J \text{ and } 1 \leq l \leq L\},$$

for each coarse subdomain τ .

Remark 3.1. Note that we impose the same random vectors for the local snapshot calculation in Equation (7) for μ_j , $j = 1, \dots, J$ in order to obtain a sparse online space.

3.2.2 Sparse local space calculations

For a given input parameter μ , we next construct the associated coarse space $V_{\text{on}}^\tau(\mu)$ for each μ value on each coarse subdomain τ . In principle, we want this to be a small dimensional subspace of the snapshot space for computational efficiency. The coarse space will be used within the finite element framework to solve the original global problem, where a continuous or discontinuous Galerkin coupling of the multiscale basis functions is used to compute the global solution. In particular, we seek a subspace of the snapshot space V_{snap}^τ such that it can approximate any element of the snapshot space in an appropriate sense. For the convenience of the presentation, we denote $\Psi_{\text{snap}}^\tau = [\psi_1^{\tau, \text{snap}}, \dots, \psi_J^{\tau, \text{snap}}]$. Similar as the generation of local snapshot space, we obtain the local sparse online basis via a local problem solved by l_1 optimization in the space of the corresponding

local snapshot space. Here, we will use a smaller subspace of V_{snap}^τ as the test space constructed through multiplication of a random matrix T_{random}^τ . Denote T_{random}^τ as a matrix of size $(L \times J)$ by q ($q \ll (L \times J)$) with rows of i.i.d standard Gaussian random vectors. Then the test space is defined as $\Psi_{\text{snap}}^\tau T_{\text{random}}^\tau$.

Specifically, the local problem is arranged as follows. Find U_l , such that, $\psi_l^{\tau,\text{on}} = \Psi_{\text{snap}}^\tau U_l$, and

$$U_l = \operatorname{argmin} \frac{1}{\nu} \|U\|_1 \quad \text{subject to } A_c(\mu)U_l = F_l. \quad (9)$$

Here, $A_c(\mu) = (\Psi_{\text{snap}}^\tau T_{\text{random}}^\tau)^T A(\mu) \Psi_{\text{snap}}^\tau$ and $F_l = (\Psi_{\text{snap}}^\tau T_{\text{random}}^\tau)^T R_l$ with $A(\mu)$ being the local stiffness matrix and R_l being the right hand side for the local problem with Dirichlet boundary condition r_l . Namely, we are solving the following local problems in V_{snap}^τ with the l_1 minimized coefficient vector U_l for the testing space equal to $\Psi_{\text{snap}}^\tau T_{\text{random}}^\tau$,

$$\begin{cases} -\operatorname{div}(\kappa(x; \mu) \nabla \psi_l^{\tau+, \text{on}}) = 0 & \text{in } \tau^+ \\ \psi_l^{\tau+, \text{on}} = r_l & \text{on } \partial\tau^+. \end{cases} \quad (10)$$

Later, we will briefly introduce the algorithm to solve Equation (9). Note that we impose the same random vectors as the boundary conditions in Equation (7) to guarantee the sparse solution in Equation (10).

We can obtain the local online snapshot functions on the target domain τ by restricting the solution of the local problem, $\psi_l^{\tau+, \text{on}}$ to τ (which is denoted by $\psi_l^{\tau, \text{on}}$). Now we are ready to present the local online snapshot space as follows,

$$V_{\text{on}}^\tau = \operatorname{Span}\{\psi_l^{\tau, \text{on}} : 1 \leq l \leq L\},$$

for each coarse subdomain τ . Then we denote $\Psi_{\text{on}}^\tau = [\psi_1^{\tau, \text{on}}, \dots, \psi_L^{\tau, \text{on}}]$.

Next we will select the dominant modes from V_{on}^τ by the following eigenvalue problem,

$$A^{\tau, \text{on}}(\mu) z_k^{\tau, \text{on}} = \lambda_k^{\tau, \text{on}} S^{\tau, \text{on}}(\mu) z_k^{\tau, \text{on}}, \quad (11)$$

where

$$A^{\tau, \text{on}}(\mu) = [a^{\text{on}}(\mu)_{mn}] = \left[\int_{\tau} \kappa(x; \mu) \nabla \psi_m^{\tau, \text{on}} \cdot \nabla \psi_n^{\tau, \text{on}} \right] = \Psi_{\text{on}}^{\tau T} A(\mu) \Psi_{\text{on}}^\tau$$

$$S^{\tau, \text{on}}(\mu) = [s^{\text{on}}(\mu)_{mn}] = \left[\int_{\tau} \kappa(x; \mu) \psi_m^{\tau, \text{on}} \psi_n^{\tau, \text{on}} \right] = \Psi_{\text{on}}^{\tau T} S(\mu) \Psi_{\text{on}}^\tau,$$

and $\kappa(x; \mu)$ is now parameter dependent. To generate the coarse space we then choose the smallest M_{on}^τ eigenvalues from Equation (11) and form the corresponding eigenvectors in R_{on}^τ by setting $\phi_k^{\tau, \text{on}} = \sum_{j=1}^L \psi_j^{\tau, \text{on}} z_{k,j}^{\tau, \text{on}}$ (for $k = 1, \dots, M_{\text{on}}^\tau$), where $z_{k,j}^{\tau, \text{on}}$ are the coordinates of the vector $\phi_k^{\tau, \text{on}}$.

Above, we presented an algorithm for solving an eigenvalue problem in the space which has a sparse representation in the snapshot space. One can attempt to obtain sparse spectral basis from Equation (10) using l_1 -minimization method in the local snapshot space V_{snap}^τ ([31, 47]). Here, we can use the algorithm proposed in [41]. The general basis pursuit problem is as follows

$$\min_{x \in \mathbb{R}^n} \|x\|_1 + \nu \|Cx - f(x)\|, \quad (12)$$

where $f \in \mathbb{R}^m$, $C \in \mathbb{R}^{m \times n}$, and $m \ll n$. We refer to [47] for the Bregman algorithm to solve (12). Instead of solving Equation (10) in the online stage, we can generate the sparse spectral basis directly following the algorithm in [41]. The first M_{on}^τ sparse spectral basis can be solved by

$$\min_{\Psi \in \mathbb{R}^{n \times M_{\text{on}}^\tau}} \frac{1}{\nu} \|\Psi\|_1 + \text{Tr}\langle \Psi^T A_c(\mu) \Psi \rangle, \text{ s.t. } \Psi^T \Psi = \text{I}. \quad (13)$$

3.2.3 Global coupling

The multiscale basis functions constructed above can be coupled via DG or CG formulation. Below, we present DG approach (similar results are observed when CG approach is used). One uses the discontinuous Galerkin (DG) approach (see also [43, 1]) to couple multiscale basis functions. This may avoid the use of the partition of unity functions; however, a global formulation needs to be chosen carefully. The global formulation is given by

$$a_{\text{DG}}(u_H^{\text{DG}}, v) = (f, v), \quad \forall v \in V_{\text{on}}, \quad (14)$$

where the bilinear form a^{DG} is defined as

$$a_{\text{DG}}(u, v) = a_H(u, v) - \sum_{E \in \mathcal{E}^H} \int_E \left(\{\kappa \nabla u \cdot n_E\} [v] + \{\kappa \nabla v \cdot n_E\} [u] \right) + \sum_{E \in \mathcal{E}^H} \frac{\gamma}{h} \int_E \bar{\kappa} [u] [v] \quad (15)$$

with

$$a_H(u, v) = \sum_{K \in \mathcal{T}_H} a_H^K(u, v), \quad a_H^K(u, v) = \int_K \kappa \nabla u \cdot \nabla v, \quad (16)$$

where $\gamma > 0$ is a penalty parameter, n_E is a fixed unit normal vector defined on the coarse edge $E \in \mathcal{E}^H$. Note that, in (15), the average and the jump operators are defined in the classical way. Specifically, consider an interior coarse edge $E \in \mathcal{E}^H$ and let K^+ and K^- be the two coarse grid blocks sharing the edge E . For a piecewise smooth function G , we define

$$\{G\} = \frac{1}{2}(G^+ + G^-), \quad \llbracket G \rrbracket = G^+ - G^-, \quad \text{on } E,$$

where $G^+ = G|_{K^+}$ and $G^- = G|_{K^-}$ and we assume that the normal vector n_E is pointing from K^+ to K^- . Moreover, on the edge E , we define $\bar{\kappa} = (\kappa_{K^+} + \kappa_{K^-})/2$ where κ_{K^\pm} is the maximum value of κ over K^\pm . For a coarse edge E lying on the boundary ∂D , we define

$$\{G\} = \llbracket G \rrbracket = G, \quad \text{and} \quad \bar{\kappa} = \kappa_K \quad \text{on } E,$$

where we always assume that n_E is pointing outside of D . We note that the DG coupling (14) is the classical interior penalty discontinuous Galerkin (IPDG) method [43] with our multiscale basis functions as the approximation space.

We can obtain the discontinuous Galerkin spectral multiscale space as

$$V_{\text{on}}^{\text{DG}}(\mu) = \text{Span}\{\phi_k^{K, \text{on}} : 1 \leq k \leq M_{\text{on}}^K, K \in \mathcal{T}^H\}. \quad (17)$$

We can obtain an operator matrix constructed by the basis functions of $V_{\text{on}}^{\text{DG}}(\mu)$. We denote the matrix as Φ_0 where $\Phi_0 = [\phi_1^{\text{DG}}, \dots, \phi_{N_c}^{\text{DG}}]$. Recall that N_c denotes the total number of coarse

basis functions. Solving the problem (2) in the coarse space $V_{\text{on}}^{\text{DG}}(\mu)$ using the DG formulation described in Equation (14) is equivalent to seeking $u_{\text{ms}}^{\text{DG}}(x; \mu) = \sum_i c_i \phi_i^{\text{DG}}(x; \mu) \in V_{\text{on}}^{\text{DG}}$ such that

$$a^{\text{DG}}(u_{\text{ms}}^{\text{DG}}, v; \mu) = (f, v) \quad \text{for all } v \in V_{\text{on}}^{\text{DG}}, \quad (18)$$

where $a^{\text{DG}}(u, v; \mu)$ and $f(v)$ are defined in Equation (15). We can obtain a coarse system

$$A_0 U_0^{\text{DG}} = F_0, \quad (19)$$

where U_0^{DG} denotes the discrete coarse DG solution, and

$$A_0(\mu) = R_0^T A(\mu) R_0 \quad \text{and} \quad F_0 = R_0^T F,$$

where $A(\mu)$ and F are the standard, fine-scale stiffness matrix and forcing vector corresponding to the form in Equation (18). After solving the coarse system, we can use the operator matrix R_0 to obtain the fine-scale solution in the form of $R_0 U_0^{\text{DG}}$.

3.2.4 Computational cost

In this section, we discuss the computational cost. For this, we assume that we have chosen J parameters, μ_1, \dots, μ_J , and L boundary conditions r_1, \dots, r_L , for constructing the snapshot space. Then, the cost for snapshot calculations will be the same as solving $J \times L$ local problems for randomized snapshots. Next, we compute the cost of solving L_{on} online randomized snapshots. Each online snapshot calculation requires solving l_1 minimization with a constraint involving $q \times (L \times J)$ matrix (see (9)). The cost of eigenvalue computation with L_{on} snapshots is considered to be small as it involves a small eigenvalue problem of the size $L_{\text{on}} \times L_{\text{on}}$. The online cost is mainly due to solving (1) solving L_{on} online randomized snapshots (2) solving a global problem on a coarse grid. The cost of solving a global problem is small if the solution has a sparse representation. As for the cost of solving online randomized snapshots, this will be small compared to solving local problems in the online stage if local problems have a high resolution. Moreover, as we pointed out earlier that the proposed approach allows a fast assembly of the stiffness matrix in the online space since it involves a few elements of the snapshot space. It also avoids using all snapshot vectors, which can result to a large dimensional representation of the online multiscale basis functions.

3.3 Second approach. Sparse Snapshot Subspace Approach

In this approach, we will use an appropriate snapshot space to compute the sparse solution directly. Again, we consider a local snapshot space $V_{\text{snap}}^\tau = \text{Span}\{\psi_i^{\tau, \text{snap}}\}$. In some applications, we may not be able to reduce the dimension of the multiscale space locally. In this case, we can use sparsity techniques directly in the global snapshot space to compute the solution. The procedure can be more expensive; however, can yield more accurate solutions. More precisely, we seek the solution in the global snapshot space of $V_{\text{snap}} = \text{Span}\{\psi_i^{\text{snap}}\}$ using l_1 minimization with testing space, V_{test} , spanned by the random combination of snapshot basis functions. This is equivalent to find $u_{\text{ms}} = \sum_i U_i^{\text{ms}} \psi_i^{\text{snap}} \in V_{\text{snap}}$ where

$$U^{\text{ms}} = \text{argmin} \|U\|_1 \quad \text{subject to} \quad a_{\text{DG}}\left(\sum_i U_i \psi_i^{\text{snap}}, v\right) = (f, v), \quad \forall v \in V_{\text{test}}. \quad (20)$$

In the following section, we will take the Helmholtz problem as an example and discuss the procedure of using this approach to compute a sparse solution. More precisely, we consider the following problem: find u such that

$$-\nabla \cdot (\kappa(x)\nabla u) - \Omega^2 n(x)u = f, \quad \text{in } D$$

with the Dirichlet boundary condition $u|_{\partial D} = g$.

3.3.1 Snapshot and test space

In this section, we present the construction of the snapshot space V_{snap} and the test space V_{test} . Since we are solving the Helmholtz equation with a fixed frequency Ω , we can assume the solution, u , can be written as a linear combination of plane waves, namely, $u = \sum_k \beta_k e^{i\Omega k \cdot x}$. Therefore, we consider our snapshot basis to be some plane waves in each coarse block $K \in \mathcal{T}^H$, that is,

$$V_{\text{snap}} = \text{Span}\{\psi_{m,j} : 1 \leq m \leq N_d \text{ and } 1 \leq j \leq M\},$$

where

$$\Psi_{m,j}(x) = \begin{cases} e^{i\Omega k_m \cdot x} & \text{for } x \in K_j \\ 0 & \text{otherwise} \end{cases} \quad (21)$$

with $k_m = (\sin(\pi m/N_d), \cos(\pi m/N_d))$, N_d as the number of propagating directions and M the number of coarse blocks. We note that the plane wave basis is not new in solving the Helmholtz equation and it was used in a number of papers (see [35, 18, 19, 45, 32] and the references therein).

Next, we will show the construction of the test space. We consider $\{r^{(l)}\}_{l=1}^{N_t}$ as a collection of i.i.d. standard Gaussian random vectors with $N_t \ll N_d$. Then the testing space V_{test} is defined by

$$V_{\text{test}} = \text{Span}\{\phi_{l,j} : \phi_{l,j} = \sum_{m=1}^{N_d} r_m^{(l)} \psi_{m,j}, 1 \leq l \leq N_t \text{ and } 1 \leq j \leq M\}.$$

Since $N_t \ll N_d$, we have a test space with dimension much smaller the snapshot space ($\dim(V_{\text{test}}) = N_t M \ll N_d M = \dim(V_{\text{snap}})$).

3.3.2 Sparse solution in the snapshot space

After constructing the snapshot and test space, we can couple the system globally by IPDG method. That is, we find $u_{\text{ms}} \in V_{\text{snap}}$ such that

$$a_{\text{DG}}(u_{\text{ms}}, v) = (f, v), \quad \forall v \in V_{\text{test}}, \quad (22)$$

where

$$a_{\text{DG}}(u, v) = a_H(u, v) - \sum_{E \in \mathcal{E}^H} \int_E \left(\{\kappa \nabla u \cdot n_E\} [v] + \{\kappa \nabla v \cdot n_E\} [u] \right) + \sum_{E \in \mathcal{E}^H} \frac{\gamma}{h} \int_E \bar{\kappa} [u] [v] \quad (23)$$

with

$$a_H(u, v) = \sum_{K \in \mathcal{T}_H} a_H^K(u, v), \quad a_H^K(u, v) = \int_K \kappa \nabla u \cdot \nabla v - \Omega^2 \int_K n(x)uv, \quad (24)$$

where $\gamma > 0$ is a penalty parameter, n_E is a fixed unit normal vector defined on the coarse edge $E \in \mathcal{E}^H$. Moreover, $\{\cdot\}$ and $[\cdot]$ are the average and jump operators defined before.

As the dimension of test space is smaller than the dimension of snapshot space, the Equation (22) does not have a unique solution. To seek for a sparse solution, we will solve a l_1 minimization problem subject to Equation (22), more precisely, we will find $u_{\text{ms}} = \sum_{l,j} U_{l,j}^{\text{ms}} \phi_{l,j} \in V_{\text{snap}}$ such that

$$U^{\text{ms}} = \operatorname{argmin}\{\|U\|_{l_1}\} \text{ subject to } a_{DG}(U_{l,j}^{\text{ms}} \phi_{l,j}, v) = (f, v), \quad \forall v \in V_{\text{test}}. \quad (25)$$

3.3.3 Cost of computations

In this section, we discuss the computational cost associated with the second approach. In this example, the cost for snapshot (plane waves) calculations is cheap as they are analytically described. In addition, the linear system in (25) has dimension $N_t M \times N_d M$, which is a highly under-determined system as $N_t \ll N_d$. Thus, one can solve the l_1 minimization problem (25) efficiently by using, for example, the Bregman's method [47]. Moreover, if an adaptivity can be used and the problem requires very few snapshot vectors or very few test vectors in many regions excepts a few coarse regions, this will increase the efficiency of the proposed approach. In this case, if we denote by $N_t^{(i)}$ and $N_d^{(i)}$ the number of test and snapshot vectors in the region i (using adaptivity), then the linear system in (25) has dimension $\left(\sum_{i=1}^M N_t^{(i)}\right) \times \left(\sum_{i=1}^M N_d^{(i)}\right)$. Thus, if $\sum_{i=1}^M N_t^{(i)}$ or $\sum_{i=1}^M N_d^{(i)}$ is not large, one can gain computational efficiency. We note that this approach is more expensive compared to the first approach, where we perform the sparsity calculations at the local coarse-grid level.

4 Numerical results

4.1 First Approach. Local-Sparse Snapshot Subspace Approach

In this section, we will present some numerical examples by using the first approach to compare the sparse multiscale solution. We consider the domain $D = [0, 1]^2$. The coarse mesh size H is $1/10$ and each coarse grid block is subdivided into a 10×10 grid, therefore, the fine mesh size $h = 1/100$;

Example 1

Setup. In our first example, we will consider the source function $f = 1$ and the medium parameter $\kappa(\mu) = (1 - \mu)\kappa_1 + \mu\kappa_2$, where κ_1 and κ_2 are shown in Figure 5. We choose the offline values of μ , $\mu_i = 0.2, 0.4, 0.6, 0.8$, for computing the online snapshot space as discussed above.

Discussions of numerical results. In Table 1, we show the convergence history of our method for $\mu = 0.5$, where we define $\|u\|_{H^1_{\kappa}(D)}^2 = \int_D \kappa |\nabla u|^2$. The fine-grid solution and the numerical solution are shown in Figure 6. First, we note that there is an irreducible error due to the use of the snapshot space, which consists of harmonic functions. This error is of order of the coarse mesh size and this is the reason, the error decay is slow (below 10 %) as we increase the dimension. In these problems, because our selected $\mu = 0.5$ is near to $\mu = 0.4$ and $\mu = 0.6$, we observe that the sparsity is close to 50 %, i.e., we only use snapshots corresponding to nearby values of μ . We observe that when the snapshot space dimension is 9600 (i.e., 24 randomized solutions per coarse block and per each value of μ_i), the nonzero coefficients in the expansion of basis functions (over the whole domain) in terms of 9600 snapshot vectors are 4850. The optimal expansion for this case

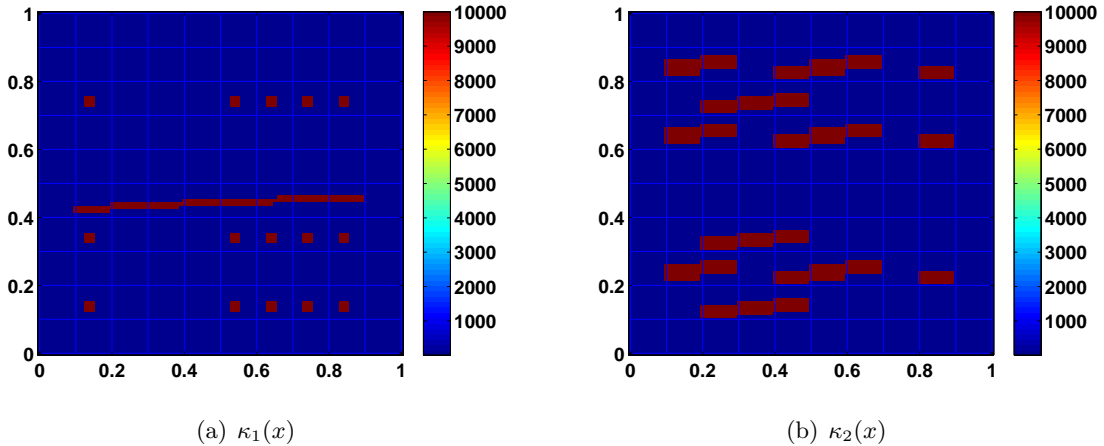


Figure 5: Decomposition of permeability field

corresponds when $\mu = 0.5$ is selected for snapshot construction and in this case, the number of nonzero coefficients is 2400 (24 per coarse region). We note that if we consider small dimensional online spaces and the full snapshot space, then the sparsity is very small. For example, if we use 12 randomized solutions per coarse block and per each value of μ_i for identifying multiscale basis functions per each coarse region, then, we will be using only 1/2 of the snapshot vectors and thus, the sparsity (the number of nonzero coefficients of the solution in the snapshot space) will be 25 %. As we observe that our numerical examples identify appropriate sparsity of the solution space. We expect a more significant gain in the sparsity if more parameter values are used.

Why to expect a sparsity. Next, we briefly describe why to expect a sparsity in this problem. Because the snapshot space consists of local problems corresponding to multiple values of μ , we expect that for an online value of μ , we will have a local (in K) coefficient $\kappa(x; \mu)$, which is similar to one of the snapshot solutions. Thus, it is more advantageous to use l_1 minimization techniques, which will select a small dimensional subspace of the snapshot space corresponding to the coefficient that is close to $\kappa(x; \mu)$ with the online value of μ . Such situations may occur in various applications. Moreover, in these examples, it is more advantageous to use local spectral decomposition and avoid a large-scale l_1 minimization problem.

Table 1: Convergence history of the DGMsFEM using oversampling Harmonic basis. The fine-scale dimension is 12100. The full snapshot space dimension is 9600.

dim(V_{on})	$\ u - u_{\text{ms}}\ $ (%)	
	$L^2(D)$	$H_{\kappa}^1(D)$
400	15.05	31.84
600	2.89	13.71
800	1.22	10.20
1000	1.12	9.83
dim(V_{snap})	1.07	9.59

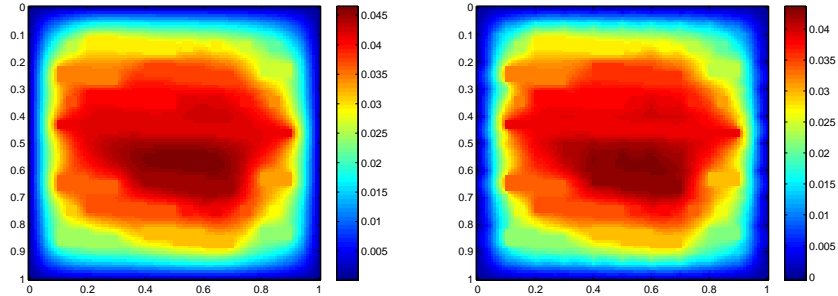


Figure 6: Left: Fine grid solution Right: Numerical solution (8 basis).

Example 2

Setup. In our second example, we consider the source function f to be the same as in the previous example. As for the medium parameter, we use a nonlinear function where the high permeability channel and inclusions move as we change the parameter. The expression for the medium parameter is

$$\kappa(\mu) = \kappa_1(x + \mu, y)$$

In Figure 7, we show four different values of μ , ($\mu = 0, 0.15, 0.3, 0.45$), that is used to construct the snapshot space. This is a complicated case as the high-conductivity region is not fixed.

Discussions of numerical results. In Table 2, we show the convergence history of our method. The fine grid solution and the numerical solution are shown in Figure 8 with $\mu = 0.14$. As we see from this table that the error is larger compared to the previous case. The error decreases as we increase the dimension of the space. However, due to the fact that we do not span all (or many) parameter values, the decay is slow. As for the sparsity, we achieve a better sparsity compared to the previous example because the online value of $\mu = 0.14$ is close to one of selected offline values $\mu = 0.15$. In fact, we observe that when the snapshot space dimension is 9600, as before, (i.e., 24 randomized solutions per coarse block and per each value of μ_i), the nonzero coefficients in the expansion of basis functions (over the whole domain) in terms of 9600 snapshot vectors are 3700. The optimal expansion for this case (i.e., the case with 24 randomized solutions per coarse block) corresponds when $\mu = 0.15$ is selected for snapshot construction and in this case, the number of nonzero coefficients is 2400 (24 per coarse region). If we consider small dimensional online spaces and the full snapshot space, then the sparsity is very small, as before. For example, if we use 6 randomized solutions per coarse block and per each value of μ_i for identifying multiscale basis functions per each coarse region, then, we will be using only 1/4 of the snapshot vectors and thus, the sparsity will be 9.5 %. As we observe that our numerical examples identify appropriate sparsity of the solution space. Again, we expect a more significant gain in the sparsity if more parameter values are used.

Remark 4.1. *We have implemented CG-GMsFEM using spectral basis approach and observed similar results.*

dim(V_{on})	$\ u - u^{\text{on}}\ $ (%)	
	$L^2(D)$	$H^1_{\kappa}(D)$
800	13.50	31.06
1000	12.02	29.45
1200	9.72	26.66
1400	7.97	24.13
dim(V_{snap})	5.78	20.27

Table 2: Convergence history of the DGMsFEM using oversampling Harmonic basis. The fine-scale dimension is 12100. The full snapshot space dimension is 9600.

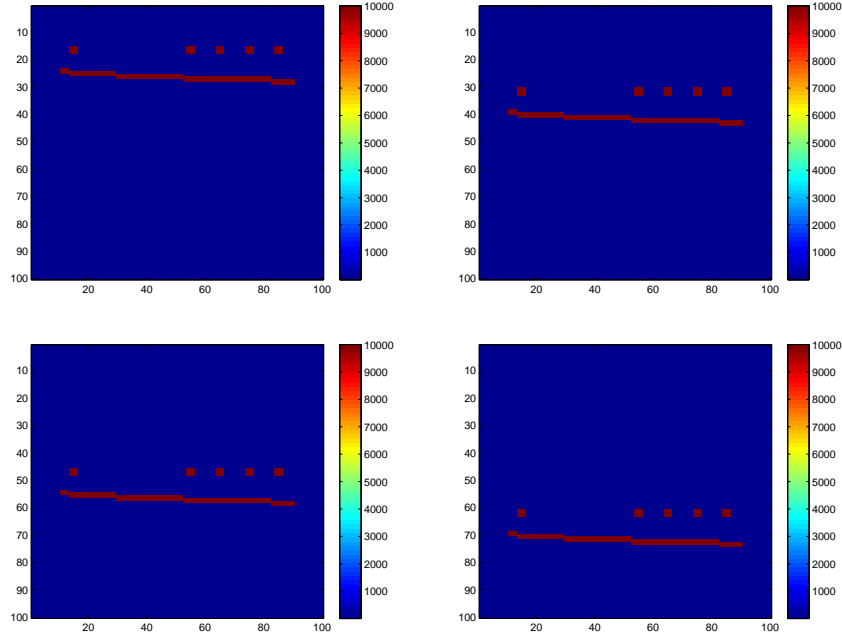


Figure 7: medium parameter. Top-Left: $\kappa(\mu_1)$, Top-Right: $\kappa(\mu_2)$, Bottom-Left: $\kappa(\mu_3)$, Bottom-Right: $\kappa(\mu_4)$

4.2 Second Approach. Sparse Snapshot Subspace Approach

In this section, we will show the numerical example by using second approach to directly calculate the sparse multiscale solution by l_1 minimization.

Example 1

Setup. In this example, we consider the domain $D = [0, 1]^2$ that is partitioned into the coarse grid with grid size $H = 1/8$ and each coarse block is subdivided into 16×16 fine square blocks with length $h = H/16$. Therefore, the fine mesh size $h = \frac{1}{128}$. We consider $\Omega = 2$, $\kappa \equiv 1$ and $n(x)$ is shown in Figure 9. We consider a zero source function with Dirichlet boundary condition g , given

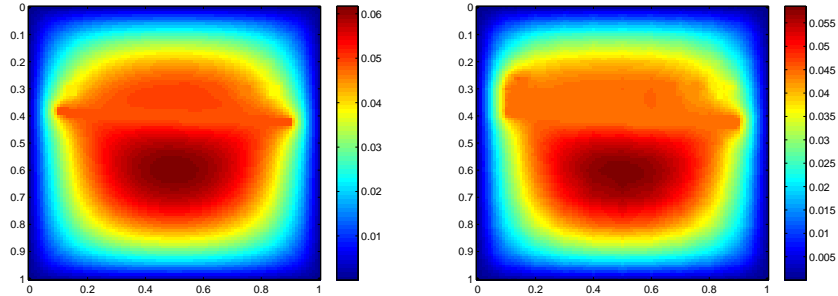


Figure 8: Left: Fine grid solution Right: Numerical solution (14 basis).

by $g = e^{-i\Omega k \cdot x}$ where $k = (\sin(\frac{\pi}{4}), \cos(\frac{\pi}{4}))$.

Discussions of numerical results. We will compare our result with the reference solution, which is calculated on the fine grid and shown in Figure 10. Notice that, within each coarse grid block, the reference solution has few dominant propagating directions, which suggests sparsity of the solution in the snapshot space. In this case, the snapshot space is spanned by local plane waves with dimension $\dim(V_{\text{snap}}) = 1280$, as defined in (21) with k_i 's distributed uniformly. The snapshot solution (i.e., if we use all snapshot vectors) has 1.63% relative error with respect to the fine-scale solution. We compare the solutions in Figure 11. As we observe, the snapshot solution is accurate. Next, we calculate the sparse solution by varying the dimension of the test space. The latter defines a sparse solution in the subspace of the test space. The numerical solution calculated with 4 test basis per coarse grid block is shown in Figure 12. In Table 3, we show the convergence history of the second approach, where $\|u\|_{H^1(D)}^2 = \int_D |\nabla u|^2$. As we observe that for low dimensional test spaces, the solution is very sparse in the snapshot space (and this sparsity is about the same as the test space). We increase the dimension of the test space to achieve a higher accuracy. For example, for the solution with the sparsity 408 (i.e., 408 non-zero coefficients in the span of 1280 snapshot vectors), we have 1.63 % L^2 error.

Why to expect a sparsity. Next, we briefly describe why to expect a sparsity in this problem. The snapshot space consists of local problems corresponding to different directions k_m (see (21)). In this problem, we expect that the solution will consist of plane wave solutions with a few directions. By using plane wave solutions, we can identify these few directions. Note that in this example, we can not identify local spectral decomposition.

$\dim(V_{\text{test}}) \times 2$	$\ u - u_{\text{ms}}\ $ (%)		sparsity of the sol
	$L^2(D)$	$H^1(D)$	
128	41.10	195.38	128
256	21.12	45.16	252
384	14.62	32.62	344
512	3.49	14.40	408
$\dim(V_{\text{snap}})$	1.63	9.88	1280

Table 3: Convergence history of the DGMsFEM to compute sparse multiscale solution directly. The fine-scale dimension is 16384. The snapshot space dimension is 1280.

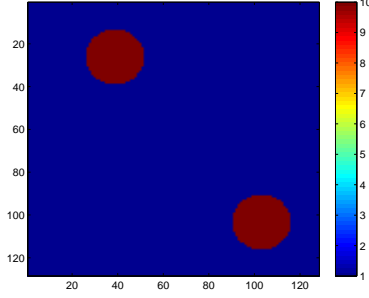


Figure 9: Parameter $n(x)$.

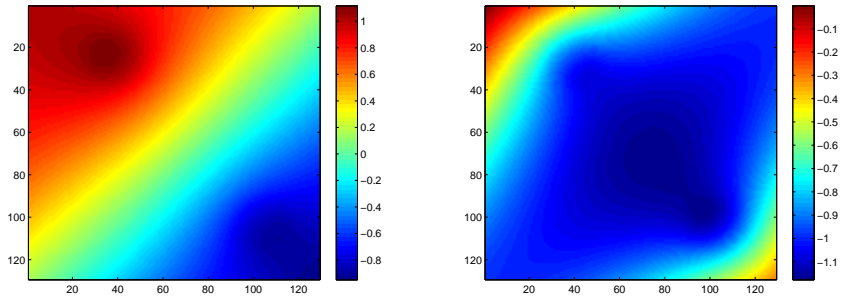


Figure 10: Reference solution u , Left: Real part of the solution; Right: Imaginary part of the solution.

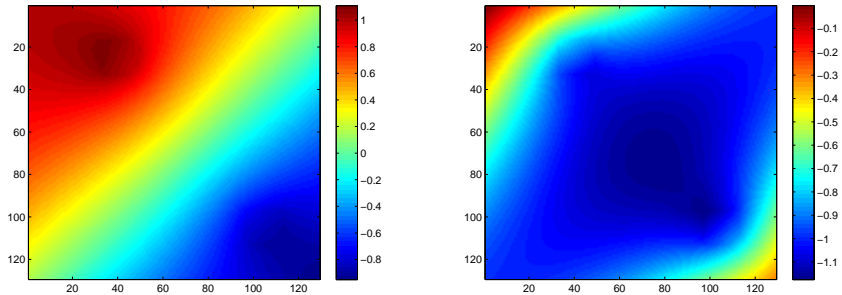


Figure 11: Snapshot solution (i.e., when using all snapshot vectors), u , Left: Real part; Right: Imaginary part.

Example 2

Setup. In this example, we consider the domain $D = [0, 1]^2$ is partitioned into the coarse grid with grid size $H = 1/16$ and each coarse block is subdivided into 16×16 fine square fine block with length $h = H/16$, therefore, the fine mesh size $h = \frac{1}{128}$. We consider $\Omega = 8$ and $n(x)$ is shown in figure 13. The parameter κ , source function f , and boundary condition g , are the same as the

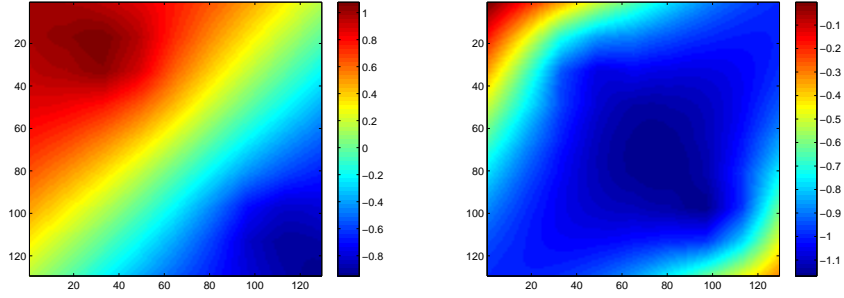


Figure 12: Numerical solution with 4 test basis functions, u , Left: Real part of the solution. Right: Imaginary part of the solution.

previous example. Because of higher value of Ω , we take the fine grid 2 times finer.

Discussions of numerical results. We will compare our results with the multiscale approach with the reference solution, which calculated on the fine grid and shown in Figure 14. Notice that, within each coarse grid block, the reference solution has few dominant propagating directions, which suggests sparsity of the solution in the snapshot space. In this case, the snapshot space is spanned by local plane waves with dimension $\dim(V_{\text{snap}}) = 5120$, as defined in (21) with k_i 's distributed uniformly. The snapshot solution error is 2.44% and it is shown in Figure 15. As we observe the snapshot solution is accurate. Next, we calculate the sparse solution by varying the dimension of the test space. The latter defines a sparse solution in the subspace of the test space. The numerical solution calculated with 4 test basis per coarse grid block is shown in Figure 16. In Table 4, we show the convergence history of the second approach. As we observe that for low dimensional test spaces, the solution is very sparse in the snapshot space. We increase the dimension of the test space to achieve a higher accuracy. For example, the solution with 1958 nonzero coefficients in the snapshot space provides 4.25 % accurate solution in L^2 sense.

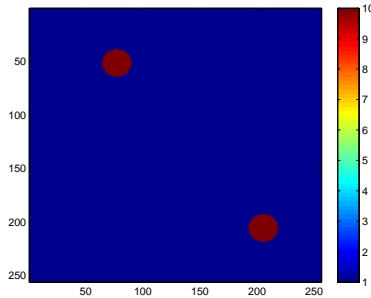


Figure 13: Parameter $n(x)$.

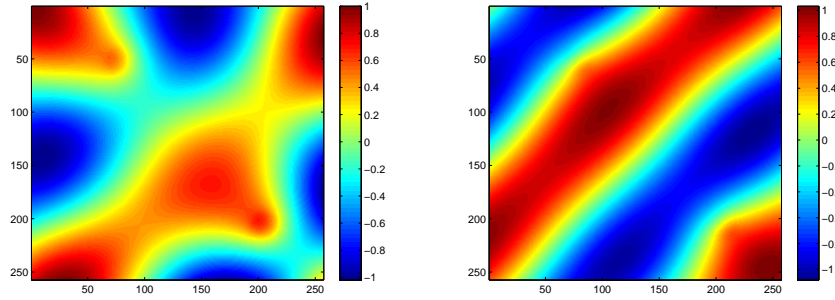


Figure 14: Reference solution u , Left: Real part of the solution; Right: Imaginary part of the solution.

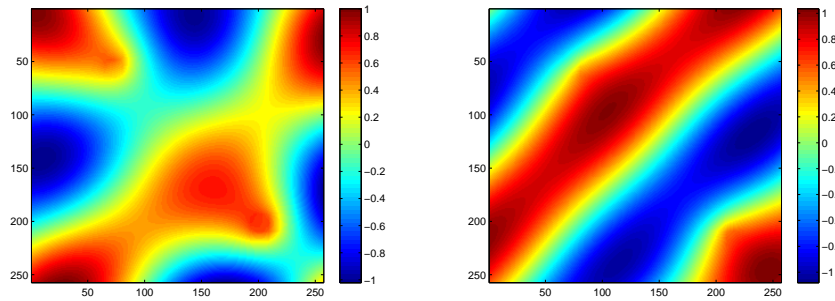


Figure 15: Snapshot solution (i.e., when using all snapshot vectors), u , Left: Real part; Right: Imaginary part.

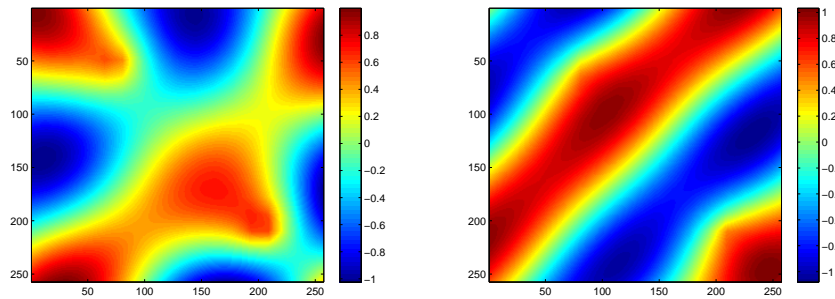


Figure 16: Numerical solution with 4 test basis functions, u , Left: Real part of the solution. Right: Imaginary part of the solution.

5 Conclusions

5.1 Summary of the results

In the paper, we develop approaches to identify sparse multiscale basis functions in the snapshot space within GMsFEM. The snapshot spaces are constructed in a special way that allows sparsity

$\dim(V_{\text{test}}) \times 2$	$\ u - u_{\text{ms}}\ $ (%)		sparsity of the sol
	$L^2(D)$	$H^1(D)$	
512	79.12	176.91	500
1024	74.07	103.93	913
1536	40.69	51.79	1294
2048	17.27	23.74	1591
2560	4.25	8.63	1958
$\dim(V_{\text{snap}})$	2.44	6.18	5120

Table 4: Convergence history of the DGMsFEM to compute sparse multiscale solution directly. The fine-scale dimension is 66049. The snapshot space dimension is 5120.

for the solution. We consider two approaches. In the first approach, local multiscale basis functions are constructed, which are sparse in the snapshot space. These multiscale basis functions are constructed by identifying dominant modes in the snapshot space using l_1 minimization techniques. As for the application, we consider parameter-dependent multiscale problems. In the second approach, we apply l_1 minimization techniques directly to solve the global problem. This approach is more expensive as it directly deals with a large snapshot space. As for the application, we consider Helmholtz equations. For both approaches and their respective applications, we present numerical results and discuss computational savings. Our numerical examples are simplistic and are designed to convey the main idea of the proposed approach.

5.2 Sparsity assumption

Both approaches assume that the solution is sparse in the snapshot space. The latter requires special snapshot spaces, which can yield this sparsity. For example, for local snapshot vectors considered in the paper, this requires identifying boundary conditions for the snapshot solutions, which can sparsely represent the solution. This may not be easy in general, though in some examples can still be achieved. Besides examples presented in the paper, one can consider scale separation cases and use piecewise linear boundary conditions. Whether a general framework for constructing these snapshot vectors is possible remains an open question.

5.3 Adaptivity and online basis functions

In general, once offline spaces are identified, we can use adaptivity [12, 9] and online basis functions [11, 10] to achieve a small error. The adaptivity is accomplished by identifying the regions with large residuals and enriching the spaces in those regions. In our earlier works [12, 9], we have shown that one needs to use some special error indicators. For the first approach, we can use the “next” eigenvector obtained from local eigenvalue decomposition to construct multiscale basis functions. For the second approach, one can increase the test space for additional multiscale basis functions.

In the regions with largest residuals, we can also use online basis functions to reduce the error substantially. Online basis functions are computed locally and identified as the localized basis functions which can give a largest reduction in the error. These basis functions involve solving local problems with a residual on the right hand side (see [10] for online basis functions for DG).

In this paper, we can apply adaptivity and online basis functions as discussed in [9, 10]. For parameter-dependent problems, one can consider identifying online basis functions for a set of μ_j 's

following the analysis in [10]. This will give a local eigenvalue problem. Another important problem for our future consideration is to identify the values of μ_1, \dots, μ_J by adaptivity.

References

- [1] D.N. Arnold, F. Brezzi, B. Cockburn, and L.D. Marini. Unified analysis of discontinuous Galerkin methods for elliptic problems. *SIAM J. Numer. Anal.*, 39(5):1749–1779, 2001/02.
- [2] Nikolai Bakhvalov and G Panasenko. *Homogenisation averaging processes in periodic media*. Springer, 1989.
- [3] M. Barrault, Y. Maday, N.C. Nguyen, and A.T. Patera. An ‘Empirical Interpolation’ Method: Application to Efficient Reduced-Basis Discretization of Partial Differential Equations. *C.R. Acad. Sci. Paris, Ser. I*, 339:667–672, 2004.
- [4] Victor M Calo, Yalchin Efendiev, Juan Galvis, and Mehdi Ghommem. Multiscale empirical interpolation for solving nonlinear pdes. *Journal of Computational Physics*, 278:204–220, 2014.
- [5] Emmanuel J Candès. The restricted isometry property and its implications for compressed sensing. *Comptes Rendus Mathématique*, 346(9):589–592, 2008.
- [6] Emmanuel J Candès et al. Compressive sampling. *Proceedings of the international congress of mathematicians*, 3:1433–1452, 2006.
- [7] Emmanuel J Candès, Justin Romberg, and Terence Tao. Robust uncertainty principles: Exact signal reconstruction from highly incomplete frequency information. *Information Theory, IEEE Transactions on*, 52(2):489–509, 2006.
- [8] S. Chaturantabut and D. C. Sorensen. Application of pod and deim to dimension reduction of nonlinear miscible viscous fingering in porous media. *Mathematical and Computer Modeling of Dynamical Systems*, 17:337–353, 2011.
- [9] Eric T Chung, Yalchin Efendiev, and Wing Tat Leung. An adaptive Generalized Multiscale Discontinuous Galerkin Method (GMsDGM) for high-contrast flow problems. *arXiv preprint arXiv:1409.3474*, 2014.
- [10] Eric T Chung, Yalchin Efendiev, and Wing Tat Leung. An online generalized multiscale discontinuous galerkin method (GMsDGM) for flows in heterogeneous media. *arXiv preprint arXiv:1504.04417*, 2015.
- [11] Eric T Chung, Yalchin Efendiev, and Wing Tat Leung. Residual-driven online generalized multiscale finite element methods. *arXiv preprint arXiv:1501.04565*, 2015.
- [12] Eric T Chung, Yalchin Efendiev, and Guanglian Li. An adaptive GMsFEM for high-contrast flow problems. *Journal of Computational Physics*, 273:54–76, 2014.
- [13] Eric T Chung, Yalchin Efendiev, Guanglian Li, and Maria Vasilyeva. Generalized multiscale finite element methods for problems in perforated heterogeneous domains. *Applicable Analysis*, to appear, 2015.

- [14] E.T. Chung, Y. Efendiev, and S. Fu. Generalized multiscale finite element method for elasticity equations. *International Journal on Geomathematics*, 5:225–254, 2014.
- [15] E.T. Chung, Y. Efendiev, and C. S. Lee. Mixed generalized multiscale finite element methods and applications. *SIAM MMS*, 13:338–366, 2015.
- [16] E.T. Chung, Y. Efendiev, and W. T. Leung. Generalized multiscale finite element method for wave propagation in heterogeneous media. *SIAM MMS*, 12:1691–1721, 2014.
- [17] E.T. Chung and W. T. Leung. A sub-grid structure enhanced discontinuous Galerkin method for multiscale diffusion and convection-diffusion problems. *Comm. Comput. Phys.*, 14:370–392, 2013.
- [18] David Colton and Peter Monk. A novel method for solving the inverse scattering problem for time-harmonic acoustic waves in the resonance region. *SIAM journal on applied mathematics*, 45(6):1039–1053, 1985.
- [19] David Colton and Peter Monk. The numerical solution of the three-dimensional inverse scattering problem for time harmonic acoustic waves. *SIAM journal on scientific and statistical computing*, 8(3):278–291, 1987.
- [20] Y. Efendiev, J. Galvis, and T. Hou. Generalized multiscale finite element methods. *Journal of Computational Physics*, 251:116–135, 2013.
- [21] Y. Efendiev, J. Galvis, G. Li, and M. Presho. Generalized multiscale finite element methods. oversampling strategies. *International Journal for Multiscale Computational Engineering*, *accepted*, 2013.
- [22] Y. Efendiev and T. Hou. *Multiscale Finite Element Methods: Theory and Applications*. Springer, 2009.
- [23] Yalchin Efendiev, Juan Galvis, R Lazarov, M Moon, and Marcus Sarkis. Generalized multiscale finite element method. symmetric interior penalty coupling. *Journal of Computational Physics*, 255:1–15, 2013.
- [24] Jacob Fish. *Practical multiscaling*. John Wiley & Sons, 2013.
- [25] Jacob Fish and Rong Fan. Mathematical homogenization of nonperiodic heterogeneous media subjected to large deformation transient loading. *International Journal for numerical methods in engineering*, 76(7):1044–1064, 2008.
- [26] J. Galvis and J. Wei. Ensemble level multiscale finite element and preconditioner for channelized systems and applications. *Journal of Computational and Applied Mathematics*, 255:456467, 2014.
- [27] Juan Galvis, Guanglian Li, and Ke Shi. A generalized multiscale finite element method for the brinkman equation. *Journal of Computational and Applied Mathematics*, 280:294–309, 2015.
- [28] K. Gao, E.T. Chung, R. Gibson, S. Fu, and Y. Efendiev. A numerical homogenization method for heterogenous, anisotropic elastic media based on multiscale theory. *Geophysics*, 80:D385–D401, 2015.

- [29] K. Gao, S. Fu, R. Gibson, E.T. Chung, and Y. Efendiev. Generalized multiscale finite element method (GMsFEM) for elastic wave propagation in heterogeneous, anisotropic media. *J. Comput. Phys.*, 295:161–188, 2015.
- [30] R. Gibson, K. Gao, E. Chung, and Y. Efendiev. Multiscale modeling of acoustic wave propagation in two-dimensional media. *Geophysics*, 79:T61–T75, 2014.
- [31] Elaine T Hale, Wotao Yin, and Yin Zhang. Fixed-point continuation for ℓ_1 -minimization: Methodology and convergence. *SIAM Journal on Optimization*, 19(3):1107–1130, 2008.
- [32] Ralf Hiptmair, Andrea Moiola, and Ilaria Perugia. Plane wave discontinuous galerkin methods for the 2d helmholtz equation: analysis of the p-version. *SIAM Journal on Numerical Analysis*, 49(1):264–284, 2011.
- [33] T. Hou and X.H. Wu. A multiscale finite element method for elliptic problems in composite materials and porous media. *J. Comput. Phys.*, 134:169–189, 1997.
- [34] Thomas Y. Hou and Pengfei Liu. A heterogeneous stochastic FEM framework for elliptic PDEs. *J. Comput. Phys.*, 281:942–969, 2015.
- [35] Tomi Huttunen and Peter Monk. The use of plane waves to approximate wave propagation in anisotropic media. *Journal of Computational Mathematics - International Edition*, 25(3):350, 2007.
- [36] P. Jenny, S.H. Lee, and H. Tchelepi. Multi-scale finite volume method for elliptic problems in subsurface flow simulation. *J. Comput. Phys.*, 187:47–67, 2003.
- [37] Yuling Jiao, Bangti Jin, and Xiliang Lu. A primal dual active set with continuation algorithm for the 0-regularized optimization problem. *Applied and Computational Harmonic Analysis*, 2014.
- [38] Alan Mackey, Hayden Schaeffer, and Stanley Osher. On the compressive spectral method. *Multiscale Modeling & Simulation*, 12(4):1800–1827, 2014.
- [39] Jens M Melenk and Ivo Babuška. The partition of unity finite element method: basic theory and applications. *Computer methods in applied mechanics and engineering*, 139(1):289–314, 1996.
- [40] H. Owhadi and L. Zhang. Metric-based upscaling. *Comm. Pure. Appl. Math.*, 60:675–723, 2007.
- [41] Vidvuds Ozolins, Rongjie Lai, Russel Caflisch, and Stanley Osher. Compressed modes for variational problems in mathematical physics and compactly supported multiresolution basis for the laplace operator. *Bulletin of the American Physical Society*, 59, 2014.
- [42] G Papanicolau, A Bensoussan, and J-L Lions. *Asymptotic analysis for periodic structures*. Elsevier, 1978.
- [43] Béatrice Rivière. *Discontinuous Galerkin methods for solving elliptic and parabolic equations: theory and implementation*. Society for Industrial and Applied Mathematics, 2008.

- [44] Hayden Schaeffer, Russel Caflisch, Cory D Hauck, and Stanley Osher. Sparse dynamics for partial differential equations. *Proceedings of the National Academy of Sciences*, 110(17):6634–6639, 2013.
- [45] Radek Tezaur and Charbel Farhat. Three-dimensional discontinuous galerkin elements with plane waves and lagrange multipliers for the solution of mid-frequency helmholtz problems. *International journal for numerical methods in engineering*, 66(5):796–815, 2006.
- [46] X.H. Wu, Y. Efendiev, and T.Y. Hou. Analysis of upscaling absolute permeability. *Discrete and Continuous Dynamical Systems, Series B.*, 2:158–204, 2002.
- [47] Wotao Yin, Stanley Osher, Donald Goldfarb, and Jerome Darbon. Bregman iterative algorithms for ℓ_1 -minimization with applications to compressed sensing. *SIAM Journal on Imaging Sciences*, 1(1):143–168, 2008.
- [48] Zhiwen Zhang, Maolin Ci, and Thomas Y. Hou. A multiscale data-driven stochastic method for elliptic PDEs with random coefficients. *Multiscale Model. Simul.*, 13(1):173–204, 2015.